Materials Today Physics 52 (2025) 101692

Contents lists available at ScienceDirect

Materials Today Physics

journal homepage: www.journals.elsevier.com/materials-today-physics

$(AgSbTe_2)_{1-x}(Bi_2Te_3)_x$-based thermoelectric device for low-grade heat recovery

Di Zhang, Min Liu, Tao Jin, Long Yang *, Wen Li **, Yanzhong Pei ***

Interdisciplinary Materials Research Center, School of Materials Science and Engineering, Tongji University, 4800 Caoan Road, Shanghai, 201804, China

ARTICLE INFO

Keywords:
$AgSbTe_2$
Thermoelectrics
Near room-temperature
Solid solution

ABSTRACT

Near room-temperature thermoelectric materials have promising applications for recovering low-grade waste heat, but high-performance *p*-type thermoelectric candidates are quite limited if compared with *n*-type ones. It is thus important to design new *p*-type materials with superior thermoelectric performance. $AgSbTe_2$ has received plenty of attention as a promising *p*-type material candidate due to its intrinsically low thermal conductivity, which is further decreased by introducing vacancies and substitutional point defects by alloying with Bi_2Te_3 in this work. With the additional help of Cd substitution at the Sb site, the optimized carrier concentration leads to a peak zT value of 0.93 at 450 K for $(AgSb_{0.98}Cd_{0.02}Te_2)_{0.9}(Bi_2Te_3)_{0.1}$, and the corresponding single-leg device achieves a conversion efficiency of ~4.2 % at a temperature gradient ΔT of ~162 K. By further pairing with an *n*-type Ag_2Se leg, a conversion efficiency of ~1.8 % is realized at a ΔT of ~93 K for the obtained module, suggesting its potential applications in the low-grade heat recovery.

1. Introduction

Thermoelectric materials enable direct conversion between thermal and electrical energy and have been used in solid-state power generation and refrigeration [1,2]. According to the figure-of-merit $zT = S^2T/\rho(\kappa_E+\kappa_L)$, high-performance thermoelectric materials are required to have high Seebeck coefficients (S), low electrical resistivities (ρ), and low electronic (κ_E) and lattice thermal conductivities (κ_L). Besides optimizing thermoelectric material properties [3,4], improving fabricated device performance plays an important role as well. For example, reducing the thermal and electrical contact losses between the material and the electrodes [5,6] as well as rationally designing the device structure [7–9] can effectively improve the energy conversion efficiency.

Bi_2Te_3-based materials have been widely used in thermoelectric cooling and power generation because of their excellent thermoelectric properties parallel to the direction of the layers [10–14]. As the dominant commercial material system for near room-temperature applications, however, its layered structure induces low mechanical performance, and it is prone to cleavage along the layer stacking direction, which is usually undesirable. Other potential alternatives such as $Mg_3(Bi, Sb)_2$ [15,16], MgAgSb [17–19], and Ag_2Se [20,21] have been continuously investigated for their power generation and cooling performance with promising applications.

Numerous efforts have been focused on the exploration of new thermoelectric materials, preferably to address the drawbacks of bismuth telluride and obtain isotropic alternatives with excellent near room-temperature properties. It is widely recognized that solid solution or doping can lead to stable structure and improve thermoelectric properties [22–26]. Meanwhile, solid solutions of different material groups may lead to novel functional materials, such as GeTe-Sb_2Te_3 solid solutions which have essential application prospects in the field of phase-change memory devices [27,28]. In addition, entropy stabilization provides a new direction for developing functional materials [29]. In the field of thermoelectricity, lattice disordering and distortions in high-entropy alloys (HEAs) tend to result in low thermal conductivity by enhancing phonon scattering [30–33].

In previous studies, the layer spacing indicator was proposed, which is based on the structural information of interlayer (spacing of layers between different planes perpendicular to the rotation symmetry axis) and intralayer (distance between nearby atoms on the same planes perpendicular to the rotation symmetry axis) [34]. It is effective in

* Corresponding author.
** Corresponding author.
*** Corresponding author.
E-mail addresses: long_yang@tongji.edu.cn (L. Yang), liwen@tongji.edu.cn (W. Li), yanzhong@tongji.edu.cn (Y. Pei).

https://doi.org/10.1016/j.mtphys.2025.101692
Received 22 January 2025; Received in revised form 1 March 2025; Accepted 5 March 2025
Available online 6 March 2025

describing the structural symmetry of materials across different crystal systems and provides a quantitative descriptor of crystal structure manipulation, in order to manipulate the electronic structure as well as electrical performance in solid solutions. It is possible to realize solid solution across the crystal structures from different crystal systems, and to obtain a certain solubility in the corresponding phase region. Following this perspective, the structural similarities between I-V-VI_2 and V_2-VI_3 materials can be established [35]. The $AgBiSe_2$ and Bi_2Te_3 single-phase solid solutions have been successfully synthesized according to this strategy, but the poor electrical properties limit their possible application scenarios [35].

$AgSbTe_2$ is a typical *p*-type I-V-VI_2 semiconductor and has been considered as a promising thermoelectric material, which can be stabilized as a cubic crystal structure at room temperature. The strong anharmonicity induced by the lone pair electrons of Sb leads to extremely low lattice thermal conductivity [36,37], while the highly degenerated bands ensure the excellent electrical transport [38,39]. A high thermoelectric performance in $AgSbTe_2$-based alloys has been frequently realized by adjusting the stoichiometric ratio of Ag/Sb [38, 40], or applying substitutions by elements such as Cd [41], Yb [42], Ti [43], and Se [44,45]. Here we applied the solid solution strategy of Bi_2Te_3-alloying, which would provide greater possibility for manipulating thermal transport properties, due to additional vacancies and defects. $AgSbTe_2$ is applied as a matrix and a series of solid solution alloys with Bi_2Te_3 are synthesized successfully. By means of this solid solution modulation with non-equiatomic anion to cation ratios, it is expected that lots of vacancies and substitutional point defects can be introduced while keeping the cubic structure skeleton unchanged, thus reducing the lattice thermal conductivity. To further improve the thermoelectric properties near room temperature, Cd was doped in the solid solution to increase the carrier concentration and thus modulate the electrical properties. The synthesized $(AgSb_{0.98}Cd_{0.02}Te_2)_{0.9}(Bi_2Te_3)_{0.1}$ exhibits $zT \approx 0.93$ at 450 K, enabling a conversion efficiency of 4.2 % at $\Delta T \sim 160$ K for $(AgSb_{0.98}Cd_{0.02}Te_2)_{0.9}(Bi_2Te_3)_{0.1}$/Co/Ag single-leg device. Furthermore, the fabrication of *p*-type $(AgSb_{0.98}Cd_{0.02}Te_2)_{0.9}(Bi_2Te_3)_{0.1}$/*n*-type Ag_2Se module presents an alternative approach for recovering low-grade heat.

2. Results and discussion

The details about material synthesis, characterizations, and property measurements are given in the Supporting Information. Room-temperature powder X-ray diffraction (XRD) patterns of $(AgSbTe_2)_{1-x}(Bi_2Te_3)_x$ are shown in Fig. 1a. The diffraction peaks of the samples at $x \leq 0.20$ provide evidence that the materials have cubic structure, whereas impurity phase precipitation of Bi_2Te_3 starts to occur at $x = 0.25$, which shows that the solid solubility is saturated at this point. The lattice constant *a* becomes larger with the increase of *x* until it stabilizes after saturation (Fig. 1b). By analyzing the crystal structures obtained by XRD Rietveld refinement (Fig. S1, Tables S1–S2), the ratio of the average layer spacing to the reference layer spacing (LS_{avg}/LS_{ref}) gradually increases with the increase of the solid solution Bi_2Te_3. This approximately linear relationship is consistent with our strategy of designing the solid solution material system.

To further validate the purity of the synthesized materials, the microstructure and composition of the samples were further characterized by scanning electron microscopy (SEM) observations and energy dispersive spectroscopy (EDS) analysis, respectively, on the samples after hot pressing. The corresponding SEM images and EDS mappings are shown in Figs. S2–S3. After exceeding the solid solubility ($x \geq 0.2$), the precipitation of heterogeneous phases is observed, which is in agreement with the XRD results. It is worth mentioning that the presence of secondary phases (silver telluride and *p*-type bismuth telluride) may affect the transport properties characterized later.

In order to reveal the thermal stability of the thermoelectric material obtained after solid solution, the results of temperature-dependent XRD for $(AgSbTe_2)_{0.9}(Bi_2Te_3)_{0.1}$ are shown in Fig. 2a. The material tends to decompose and fails to maintain a stable cubic structure at 475 K while it is completely denatured by 600 K. Detailed Rietveld refinement results of temperature-dependent XRD data are shown in Fig. S4 and Table S3. Furthermore, the resistivity of the material is tested during heating and cooling, and the maximum test temperature is sequentially increased by 20 K for each time. It changed negligibly within 460 K (Fig. 2b). The detailed characterization before and after annealing can be found in Fig. S5. These results reveal that the material properties can maintain a stable response in this temperature region. Therefore, the investigation of the transport properties of the solid solutions is focused on the temperature range of 300–450 K.

The detailed thermoelectric properties of the solid solution are shown in Fig. S6. As the solid solution content of Bi_2Te_3 increases, a growing number of vacancies are introduced into the pristine stable cubic lattice, and the lattice thermal conductivity (κ_L) basically exhibits an effective decrease due to various phonon scattering mechanisms such as dislocation scattering and interface scattering [46–49]. The sudden increase in thermal conductivity for the sample with $x = 0.2$ is presumably due to the Bi_2Te_3 precipitation, which has higher thermal conductivity than $AgSbTe_2$, in agreement with the SEM results of Fig. S2. The optical measurement (Fig. S7) shows an estimated band gap of $\approx$ 0.44 eV for $(AgSbTe_2)_{0.9}(Bi_2Te_3)_{0.1}$, which is close to $AgSbTe_2$, exhibiting a semiconductor characteristic. The thermal conductivity of $(AgSbTe_2)_{0.9}(Bi_2Te_3)_{0.1}$ is obviously decreased compared to the intrinsic $AgSbTe_2$ due to the introduction of vacancies and substitutional point defects during the solid solution, where the electrical properties can be optimized by adjusting the carrier concentration, in order to further

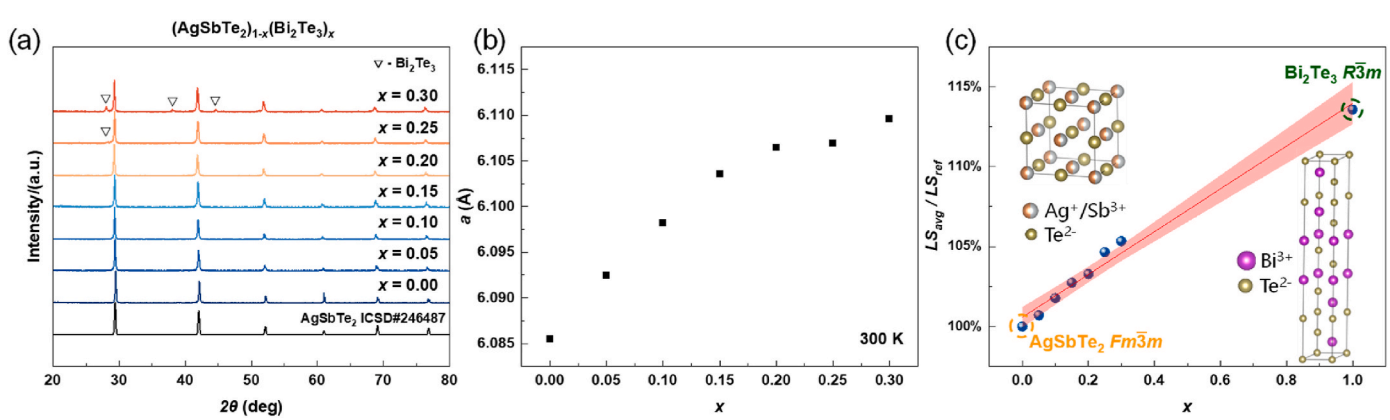

Fig. 1. (a) Room-temperature powder X-ray diffraction (XRD) patterns, (b) composition-dependent lattice parameters, and (c) the relationship between the close-packed layer spacing ratio (LS_{avg}/LS_{ref}) for $(AgSbTe_2)_{1-x}(Bi_2Te_3)_x$ ($0 \leq x \leq 0.30$).

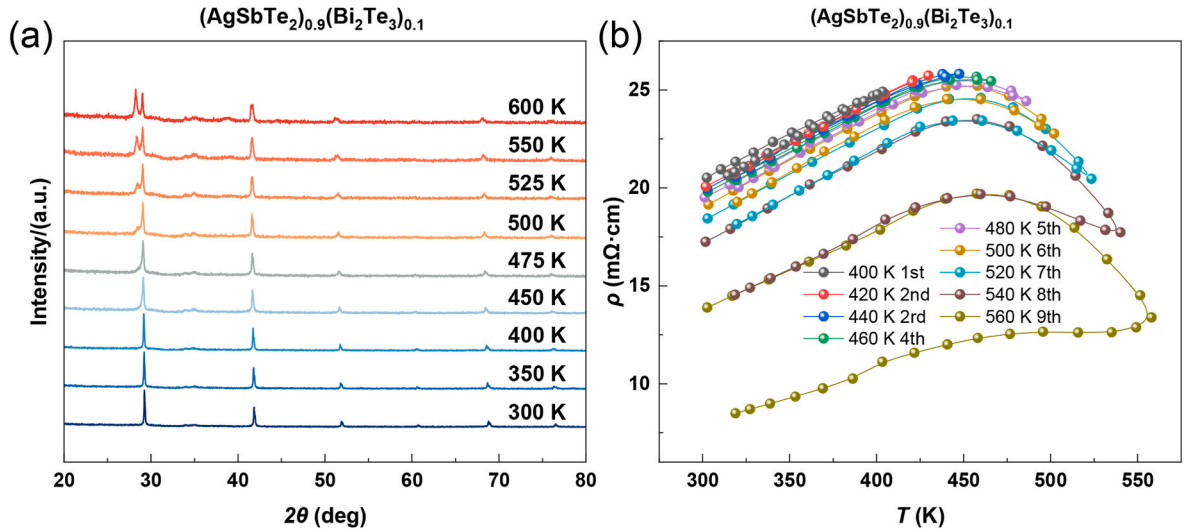

Fig. 2. (a) Temperature-dependent XRD and (b) resistivity during several thermal cycles of $(AgSbTe_2)_{0.9}(Bi_2Te_3)_{0.1}$.

improve the overall performance.

It is well known that doping with heterovalent elements is an effective method of tuning carrier concentrations. From literature reports, the doping of Cd can greatly improve the electrical and thermal properties in $AgSbTe_2$ [41]. As illustrated in Fig. S8, the XRD patterns of the $(AgSb_{1-y}Cd_yTe_2)_{0.9}(Bi_2Te_3)_{0.1}$ ($0 \leq y \leq 0.04$) samples and the SEM-EDS mapping results demonstrate that the rock-salt cubic structure was obtained successfully. The temperature-dependent thermoelectric property after Cd doping is shown in Fig. 3. The hole concentration is increased, due to the substitution of Cd for Sb, and accordingly, the Seebeck coefficient and resistivity are significantly reduced, indicating the effectiveness of Cd doping. The Pisarenko curves and the effective mass of the density of states m^* based on the single parabolic band model with acoustic scattering at 300 K are supplemented in Fig. S9 and Table S4. Benefiting from the intrinsically low κ_L and the improved electronic properties by Cd doping, the peak zT value of 0.93 is achieved at 450 K. The sample with $y = 0.04$ was not considered due to the presence of a weak CdTe second phase. The results show that $(AgSb_{0.98}Cd_{0.02}Te_2)_{0.9}(Bi_2Te_3)_{0.1}$ is a promising p-type thermoelectric candidate for low-temperature applications.

The $(AgSb_{0.98}Cd_{0.02}Te_2)_{0.9}(Bi_2Te_3)_{0.1}$/Co/Ag single-leg device and module were fabricated to illustrate the potential of the designed thermoelectric material for efficient and robust power generation application. Numerous studies have shown that an excellent interface is an

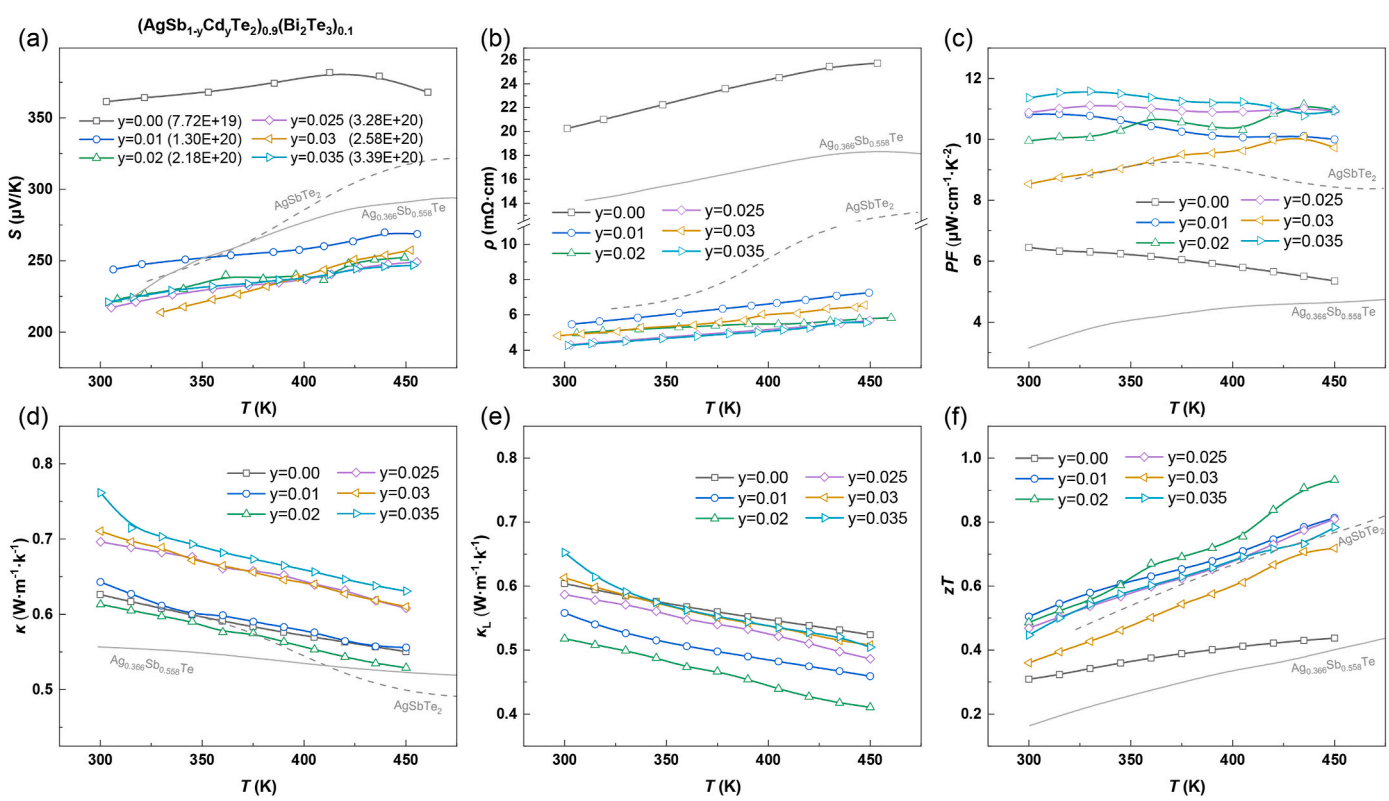

Fig. 3. Temperature-dependent (a) Seebeck coefficient, (b) resistivity, (c) power factor (PF), (d) total thermal conductivity (κ), (e) lattice thermal conductivity, and (f) thermoelectric figure-of-merit for $(AgSb_{1-y}Cd_yTe_2)_{0.9}(Bi_2Te_3)_{0.1}$ ($0 \leq y \leq 0.035$), with a comparison to those of $AgSbTe_2$ [50] and $Ag_{0.366}Sb_{0.558}Te$ [38].

important factor to determine the device output [6,16,51–53]. The interfacial electrical/thermal contact resistance, the bond strength and degree of interdiffusion between the barrier layer, and the thermoelectric material highly affect the efficiency and lifetime of the device. In this work, Co was chosen as the diffusion barrier layer and Ag as the electrode with $(AgSb_{0.98}Cd_{0.02}Te_2)_{0.9}(Bi_2Te_3)_{0.1}$ based thermoelectric material. As shown in Fig. 4, Co layer is well bonded to $(AgSb_{0.98}Cd_{0.02}Te_2)_{0.9}(Bi_2Te_3)_{0.1}$ thermoelectric material and Ag electrodes, with negligible diffusion/reaction, and the thickness of Co diffusion barrier layer is ~120 μm. The electrical contact resistance (R_c), including both electrode and diffusion barrier, of $(AgSb_{0.98}Cd_{0.02}Te_2)_{0.9}(Bi_2Te_3)_{0.1}$/Co/Ag is estimated to be ~3.4 mΩ, and the total contact resistance at both cold and hot sides accounts for approximately 7 % of the internal resistance (R_{in}) of the single-leg device, suggesting good interfacial contacts (Fig. 4b and c). This corresponds to an average interfacial contact resistivity (ρ_c) of ~131 μΩ cm^2.

The schematics of the device performance measurement in this work are shown in Fig. S10. With a fixed cold-side temperature of ~290 K, the open circuit voltage V_{OC}, maximum output power P_{max}, and maximum conversion efficiency η_{max} versus temperature gradients (ΔT) for the $(AgSb_{0.98}Cd_{0.02}Te_2)_{0.9}(Bi_2Te_3)_{0.1}$/Co/Ag single-leg device and $(AgSb_{0.98}Cd_{0.02}Te_2)_{0.9}(Bi_2Te_3)_{0.1}/Ag_2Se$ modules are shown in Fig. 5 and Figs. S11–S12. The slopes of the *V-I* curves represent the internal resistance of devices. The output power and conversion efficiency increase with current at different ΔT and reach the maximum values (Fig. 5, S11-S12). For the single-leg device, P and η increase with ΔT increasing from 27 K to 162 K, reaching the maximum values of ~5.6 mW and 4.2 % at $\Delta T = 162$ K (hot-side temperature $T_h = 453$ K, cold-side temperature $T_c = 291$ K), respectively, as shown in Fig. 5a and b. Note that the conversion efficiency measurements of the $(AgSb_{0.98}Cd_{0.02}Te_2)_{0.9}(Bi_2Te_3)_{0.1}/Ag_2Se$ modules were carried out under 380 K to avoid the phase transition in Ag_2Se at 406 K [54]. The measured voltage V, P, and η as a function of current I for two $(AgSb_{0.98}Cd_{0.02}Te_2)_{0.9}(Bi_2Te_3)_{0.1}/Ag_2Se$ modules at different ΔT are presented in Fig. 5 and Fig. S12. It suggests that the power generation performance of the two modules coincides very well in Fig. S12. P_{max} and η_{max} increase as ΔT increases, P_{max} reaches 21 mW at the $\Delta T = 93$ K, and η_{max} is 1.8 % of the $(AgSb_{0.98}Cd_{0.02}Te_2)_{0.9}(Bi_2Te_3)_{0.1}/Ag_2Se$ modules (Fig. 5a and b). This gives a new pairing possibility for Bi_2Te_3-free power generation modules.

The measurements of several thermal cycles within a temperature range of 290–453 K, as shown in Figs. S11m–p, indicate excellent thermal stability for the $AgSbTe_2$-based single-leg device. While slight decreases in η_{max} and P_{max} are still observed during the long-term stability measurements (Fig. 6), this phenomenon can be reasonably understood by the increased interfacial contact resistivity, since the nearly unchanged V_{oc} elucidates the thermal stability of the thermoelectric material at the hot-side temperature of 446 K.

3. Conclusion

In summary, the cubic $AgSbTe_2$ material was selected as the matrix to explore new *p*-type thermoelectric material candidates for near room-temperature applications. Following the 'layer stacking indicator'

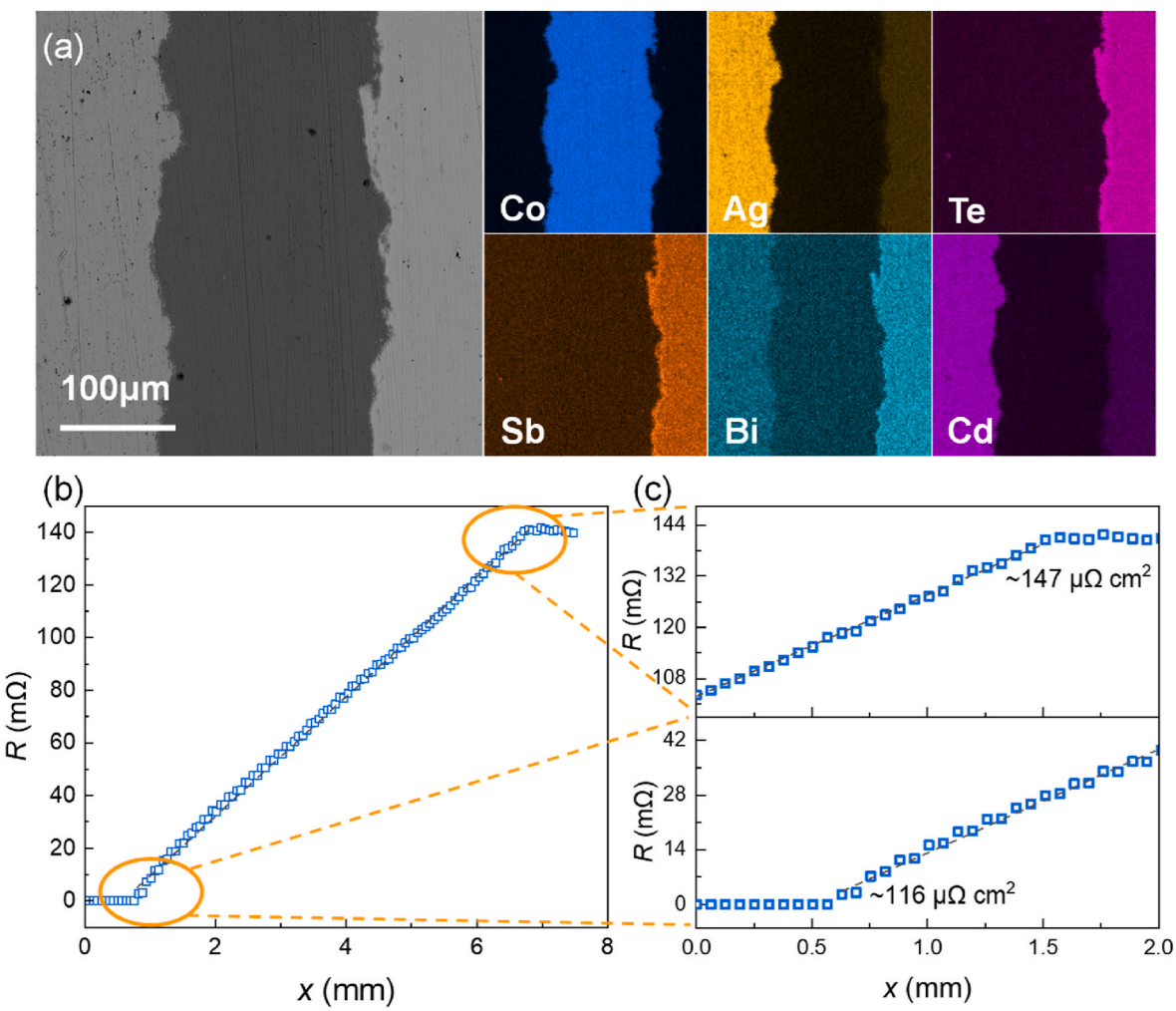

Fig. 4. (a) SEM imaging and the corresponding EDS mapping results, (b, c) line scan resistance (R) at the $(AgSb_{0.98}Cd_{0.02}Te_2)_{0.9}(Bi_2Te_3)_{0.1}$/Co/Ag interfaces.

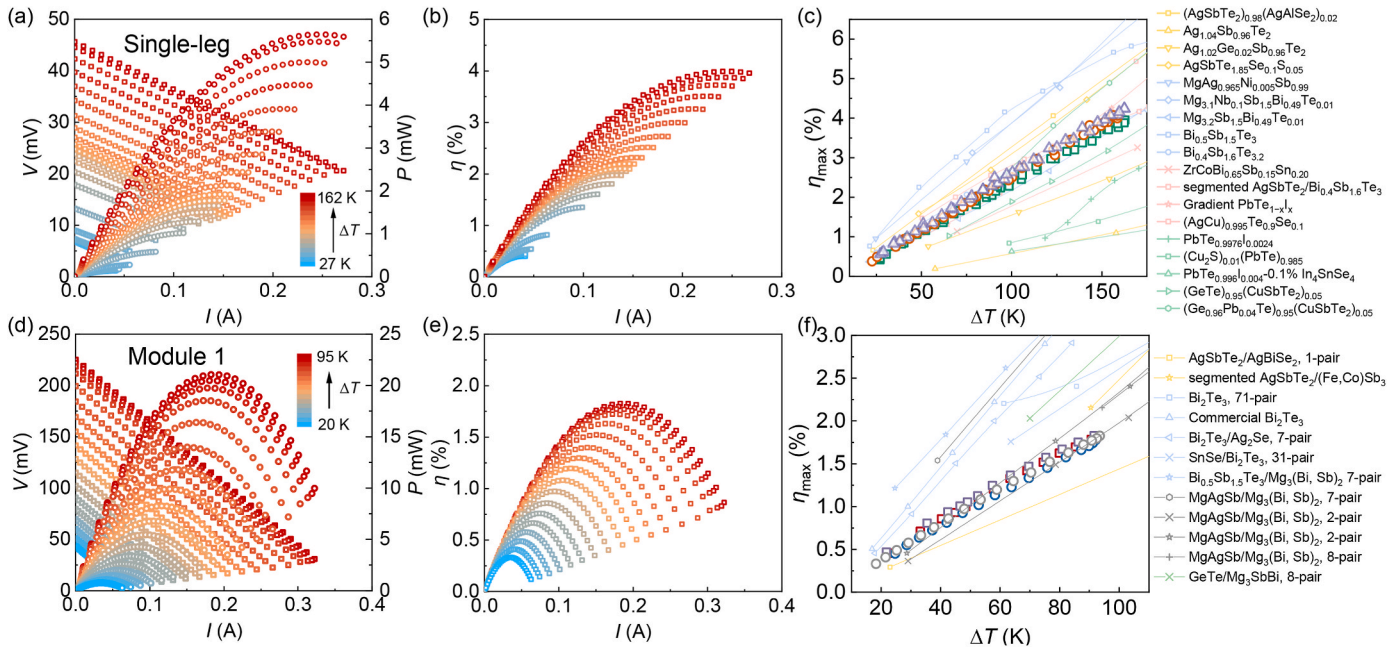

Fig. 5. Power generation performance of (a–c) $(AgSb_{0.98}Cd_{0.02}Te_2)_{0.9}(Bi_2Te_3)_{0.1}$/Co/Ag single-leg and (d–f) $(AgSb_{0.98}Cd_{0.02}Te_2)_{0.9}(Bi_2Te_3)_{0.1}/Ag_2Se$ module. (a, d) Output voltage V and output power P, (b, e) conversion efficiency η versus input current I at different temperature gradients (ΔT). (c, f) Maximum conversion efficiency η_{max} as a function of temperature gradients (ΔT). Literature results are included for comparison [5,6,15,19,20,44,50,53,55–70].

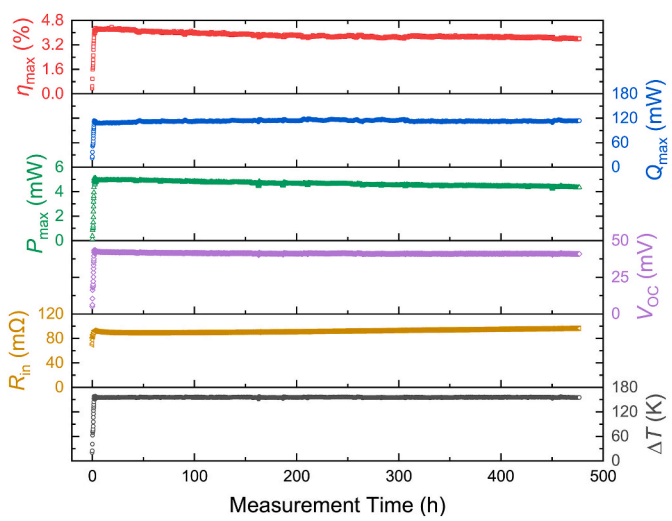

Fig. 6. Maximum conversion efficiency (η_{max}), maximum heat flow (Q_{max}), maximum output power (P_{max}), open circuit voltage (V_{OC}), internal resistance (R_{in}), and temperature gradients (ΔT) for the $(AgSb_{0.98}Cd_{0.02}Te_2)_{0.9}(Bi_2Te_3)_{0.1}$/Co/Ag single-leg device during the long-term measurements.

between crystal systems, new $AgSbTe_2$-Bi_2Te_3 solid solutions were obtained. The thermal conductivity of the system is reduced effectively and excellent thermal stability below 450 K is validated in continuous cycling tests. By further adjusting the carrier concentration, the peak zT value of 0.93 was achieved in $(AgSb_{0.98}Cd_{0.02}Te_2)_{0.9}(Bi_2Te_3)_{0.1}$. The corresponding $(AgSb_{0.98}Cd_{0.02}Te_2)_{0.9}(Bi_2Te_3)_{0.1}$/Co/Ag single-leg device shows the interfacial contact resistivity of ~131 μΩ cm^2. The p-type $(AgSb_{0.98}Cd_{0.02}Te_2)_{0.9}(Bi_2Te_3)_{0.1}$/Co/Ag single-leg device shows a maximum conversion efficiency of 4.2 % operating at a temperature gradient ΔT of 162 K, and the p-$(AgSb_{0.98}Cd_{0.02}Te_2)_{0.9}(Bi_2Te_3)_{0.1}$/$n$-$Ag_2Se$ module exhibits the efficiency of 1.8 % at $\Delta T = 93$ K. This solid solution strategy provides new opportunities to search for promising thermoelectric candidates for near room-temperature applications and to explore advanced new materials for low-grade heat recovery. More novel p/n-type thermoelectric material systems may be explored in future investigations to further expand the thermoelectric candidates.

CRediT authorship contribution statement

Di Zhang: Writing – original draft, Visualization, Validation, Methodology, Investigation, Data curation. **Min Liu:** Validation, Methodology, Data curation. **Tao Jin:** Validation, Methodology. **Long Yang:** Writing – review & editing, Visualization, Validation. **Wen Li:** Writing – review & editing, Visualization, Validation. **Yanzhong Pei:** Writing – review & editing, Visualization, Validation.

Declaration of competing interest

The authors declare that they have no known competing financial interests or personal relationships that could have appeared to influence the work reported in this paper.

Acknowledgements

This work is supported by the National Natural Science Foundation of China (Grant No. T2125008, 52371234, 92263108, 52302193), the Hong Kong, Macao and Taiwan Science and Technology Cooperation Project for Science and Technology Innovation Plan of Shanghai (23520760600) and the Fundamental Research Funds for the Central Universities.

Appendix A. Supplementary data

Supplementary data to this article can be found online at https://doi.org/10.1016/j.mtphys.2025.101692.

Data availability

Data will be made available on request.

References

[1] S.M. Pourkiaei, M.H. Ahmadi, M. Sadeghzadeh, S. Moosavi, F. Pourfayaz, L. Chen, M.A. Pour Yazdi, R. Kumar, Thermoelectric cooler and thermoelectric generator devices: a review of present and potential applications, modeling and materials, Energy 186 (2019): 115849.

[2] Y. Qin, B. Qin, D. Wang, C. Chang, L.-D. Zhao, Solid-state cooling: thermoelectrics, Energy Environ. Sci. 15 (11) (2022) 4527–4541.

[3] Z.L. Bu, X.Y. Zhang, B. Shan, J. Tang, H.X. Liu, Z.W. Chen, S.Q. Lin, W. Li, Y.Z. Pei, Realizing a 14% single-leg thermoelectric efficiency in GeTe alloys, Sci. Adv. 7 (19) (2021).

[4] M. Hong, M. Li, Y. Wang, X.L. Shi, Z.G. Chen, Advances in versatile GeTe thermoelectrics from materials to devices, Adv. Mater. 35 (2) (2023): 2208272.

[5] M. Liu, W. Li, Y. Pei, Screening metal diffusion barriers for thermoelectric $Bi_{0.5}Sb_{1.5}Te_3$, Sci. China Mater. 67 (1) (2024) 289–294.

[6] M. Liu, X. Zhang, J. Tang, Z. Chen, W. Li, Y. Pei, Screening metallic diffusion barriers for weldable thermoelectric devices, Science Bulletin 68 (21) (2023) 2536–2539.

[7] W. Zhou, K. Pang, Z. Zhang, H. Yang, Q. Zhang, Y. Li, Y. Zhang, H. Hu, X. Tan, P. Sun, et al., Optimized thermoelectric cooler performance by the structure-matching design of asymmetrical p/n-Type legs, ACS Appl. Mater. Interfaces 15 (48) (2023) 56064–56071.

[8] J. Mao, G. Chen, Z. Ren, Thermoelectric cooling materials, Nat. Mater. 20 (4) (2021) 454–461.

[9] L. Zhao, D. Liu, J. Feng, E. Min, J. Li, Y. Ling, H. Li, D. Zhao, R. Liu, R. Sun, Simultaneous optimization of cooling temperature difference and efficiency for multi-stage thermoelectric device, Appl. Energy 373 (2024): 123878.

[10] Y. Li, S. Bai, Y. Wen, Z. Zhao, L. Wang, S. Liu, J. Zheng, S. Wang, S. Liu, D. Gao, et al., Realizing high-efficiency thermoelectric module by suppressing donor-like effect and improving preferred orientation in n-type $Bi_2(Te, Se)_3$, Science Bulletin 69 (11) (2024) 1728–1737.

[11] R. Deng, X. Su, S. Hao, Z. Zheng, M. Zhang, H. Xie, W. Liu, Y. Yan, C. Wolverton, C. Uher, et al., High thermoelectric performance in $Bi_{0.46}Sb_{1.54}Te_3$ nanostructured with ZnTe, Energy Environ. Sci. 11 (6) (2018) 1520–1535.

[12] G. Wu, Q. Zhang, X. Tan, Y. Fu, Z. Guo, Z. Zhang, Q. Sun, Y. Liu, H. Shi, J. Li, et al., Bi_2Te_3-Based thermoelectric modules for efficient and reliable low-grade heat recovery, Adv. Mater. 36 (26) (2024): 2400285.

[13] G. Yang, L. Sang, F.F. Yun, D.R.G. Mitchell, G. Casillas, N. Ye, K. See, J. Pei, X. Wang, J.-F. Li, et al., Significant enhancement of thermoelectric figure of merit in BiSbTe-based composites by incorporating carbon microfiber, Adv. Funct. Mater. 31 (15) (2021): 2008851.

[14] G. Wu, Q. Zhang, Y. Fu, X. Tan, J.G. Noudem, Z. Zhang, C. Cui, P. Sun, H. Hu, J. Wu, et al., High-efficiency thermoelectric module based on high-performance $Bi_{0.42}Sb_{1.58}Te_3$ materials, Adv. Funct. Mater. 33 (47) (2023): 2305686.

[15] N. Chen, H. Zhu, G. Li, Z. Fan, X. Zhang, J. Yang, T. Lu, Q. Liu, X. Wu, Y. Yao, et al., Improved figure of merit (z) at low temperatures for superior thermoelectric cooling in $Mg_3(Bi,Sb)_2$, Nat. Commun. 14 (1) (2023) 4932.

[16] J. Yang, G. Li, H. Zhu, N. Chen, T. Lu, J. Gao, L. Guo, J. Xiang, P. Sun, Y. Yao, et al., Next-generation thermoelectric cooling modules based on high-performance $Mg_3(Bi,Sb)_2$ material, Joule 6 (1) (2022) 193–204.

[17] H. Zhao, J. Sui, Z. Tang, Y. Lan, Q. Jie, D. Kraemer, K. McEnaney, A. Guloy, G. Chen, Z. Ren, High thermoelectric performance of MgAgSb-based materials, Nano Energy 7 (2014) 97–103.

[18] X. Zhang, N. Chen, K. Guo, Q. Zhang, Q. Zhao, J. Xu, H. Zhu, H. Zhao, High cooling and power generation performance of α-MgAgSb with intrinsic low lattice thermal conductivity, Materials Today Physics 44 (2024): 101451.

[19] X. Zhang, H. Zhu, X. Dong, Z. Fan, Y. Yao, N. Chen, J. Yang, K. Guo, J. Hao, L. He, et al., High-performance $MgAgSb/Mg_3(Sb,Bi)_2$-based thermoelectrics with $\eta = 12\%$ at $T \leq 583K$, Joule 8 (12) (2024) 3324–3335.

[20] M. Liu, X. Zhang, S. Zhang, Y. Pei, Ag_2Se as a tougher alternative to n-type Bi_2Te_3 thermoelectrics, Nat. Commun. 15 (1) (2024) 6580.

[21] D. Yang, X.-L. Shi, M. Li, M. Nisar, A. Mansoor, S. Chen, Y. Chen, F. Li, H. Ma, G. X. Liang, et al., Flexible power generators by Ag_2Se thin films with record-high thermoelectric performance, Nat. Commun. 15 (1) (2024) 923.

[22] J. Li, X.Y. Zhang, Z.W. Chen, S.Q. Lin, W. Li, J.H. Shen, I.T. Witting, A. Faghaninia, Y. Chen, A. Jain, et al., Low-symmetry rhombohedral GeTe thermoelectrics, Joule 2 (5) (2018) 976–987.

[23] H.-X. Liu, X.-Y. Zhang, Z.-L. Bu, W. Li, Y.-Z. Pei, Thermoelectric properties of $(GeTe)_{1-x}[(Ag_2Te)_{0.4}(Sb_2Te_3)_{0.6}]_x$ alloys, Rare Met. 41 (3) (2022) 921–930.

[24] D. Sarkar, S. Roychowdhury, R. Arora, T. Ghosh, A. Vasdev, B. Joseph, G. Sheet, U. V. Waghmare, K. Biswas, Metavalent bonding in GeSe leads to high thermoelectric performance, Angew. Chem. Int. Ed. 60 (18) (2021) 10350–10358.

[25] N. Li, G. Wang, Z. Zhou, G. Wang, G. Han, X. Lu, X. Zhou, IV-VI/I-V-VI_2 thermoelectrics: recent progress and perspectives, Adv. Funct. Mater. 34 (44) (2024): 2405158.

[26] Y. Wang, B. Qin, T. Hong, L. Su, X. Gao, D. Wang, L.-D. Zhao, Enhanced thermoelectric performance in cubic form of SnSe stabilized through enformatingly alloying $AgSbTe_2$, Acta Mater. 227 (2022): 117681.

[27] C. Lee, D. Kim, H. Lim, Y. Seong, H. Kim, J.H. Park, D. Yang, H.J. Shin, M. Wuttig, B.J. Choi, M.-H. Cho, Ultrahigh stability and operation performance in Bi-doped $GeTe/Sb_2Te_3$ superlattices achieved by tailoring bonding and structural properties, ACS Nano 18 (37) (2024) 25625–25635.

[28] B. Sa, J. Zhou, Z. Sun, J. Tominaga, R. Ahuja, Topological insulating in $GeTe/Sb_2Te_3$ phase-change superlattice, Phys. Rev. Lett. 109 (9) (2012): 096802.

[29] N. Dragoe, D. Bérardan, Order emerging from disorder, Science 366 (6465) (2019) 573–574.

[30] B.B. Jiang, Y. Yu, J. Cui, X.X. Liu, L. Xie, J.C. Liao, Q.H. Zhang, Y. Huang, S.C. Ning, B.H. Jia, et al., High-entropy-stabilized chalcogenides with high thermoelectric performance, Science 371 (6531) (2021), 830-+.

[31] J.L. Braun, C.M. Rost, M. Lim, A. Giri, D.H. Olson, G.N. Kotsonis, G. Stan, D. W. Brenner, J.-P. Maria, P.E. Hopkins, Charge-induced disorder controls the thermal conductivity of entropy-stabilized oxides, Adv. Mater. 30 (51) (2018): e1805004.

[32] L. Hu, Y. Zhang, H. Wu, J. Li, Y. Li, M. McKenna, J. He, F. Liu, S.J. Pennycook, X. Zeng, Entropy engineering of SnTe: multi-principal-element alloying leading to ultralow lattice thermal conductivity and state-of-the-art thermoelectric performance, Adv. Energy Mater. 8 (29) (2018): 1802116.

[33] B. Jiang, P. Qiu, H. Chen, J. Huang, T. Mao, Y. Wang, Q. Song, D. Ren, X. Shi, L. Chen, Entropy optimized phase transitions and improved thermoelectric performance in n-type liquid-like Ag_9GaSe_6 materials, Materials Today Physics 5 (2018) 20–28.

[34] T. Jin, L. Yang, X.Y. Zhang, W. Li, Y.Z. Pei, Close-packed layer spacing as a practical guideline for structure symmetry manipulation of IV-VI/I-V-VI_2 thermoelectrics, InfoMat 6 (2) (2023): e12502.

[35] T. Jin, L. Yang, D. Zhang, X. Yang, X. Zhang, T. Kang, B. Ge, P. Nan, W. Li, Y. Pei, Designing semiconductors from the assembly of close-packed slabs, Chem. Mater. 36 (22) (2024) 11189–11199.

[36] D.T. Morelli, V. Jovovic, J.P. Heremans, Intrinsically minimal thermal conductivity in cubic I-V-VI_2 semiconductors, Phys. Rev. Lett. 101 (3) (2008): 035901.

[37] L.H. Ye, K. Hoang, A.J. Freeman, S.D. Mahanti, J. He, T.M. Tritt, M.G. Kanatzidis, First-principles study of the electronic, optical, and lattice vibrational properties of $AgSbTe_2$, Phys. Rev. B 77 (24) (2008): 245203.

[38] H.X. Liu, W. Li, H.W. Shen, X.Y. Zhang, S.Q. Lin, Y.Z. Pei, Evaluation of thermoelectric properties of $Ag_{0.366}Sb_{0.558}Te$, Ann. Phys. 532 (11) (2020): 1900561.

[39] T. Ghosh, S. Roychowdhury, M. Dutta, K. Biswas, High-performance thermoelectric energy conversion: a tale of atomic ordering in $AgSbTe_2$, ACS Energy Lett. 6 (8) (2021) 2825–2837.

[40] Y. Wu, Q. Liang, X. Zhao, H. Wu, P. Zi, Q. Tao, L. Yu, X. Su, J. Wu, Z. Chen, et al., Enhancing thermoelectric performance of $AgSbTe_2$-based compounds via microstructure modulation combining with entropy engineering, ACS Appl. Mater. Interfaces 14 (2) (2022) 3057–3065.

[41] S. Roychowdhury, T. Ghosh, R. Arora, M. Samanta, L. Xie, N.K. Singh, A. Soni, J. Q. He, U.V. Waghmare, K. Biswas, Enhanced atomic ordering leads to high thermoelectric performance in $AgSbTe_2$, Science 371 (6530) (2021) 722–727.

[42] V. Taneja, S. Das, K. Dolui, T. Ghosh, A. Bhui, U. Bhat, D.K. Kedia, K. Pal, R. Datta, K. Biswas, High thermoelectric performance in phonon-glass electron-crystal like $AgSbTe_2$, Adv. Mater. 36 (6) (2024): 2307058.

[43] X. Hu, S.K. Zheng, Q.H. Xiong, S. Wu, Y.L. Huang, B. Zhang, W. Wang, X.C. Wang, N.H. Li, Z.Z. Zhou, et al., Enhancement on thermoelectric performance by Ti doping and vacancies, Materials Today Physics 38 (2023): 101255.

[44] Y. Zhang, Z. Li, S. Singh, A. Nozariasbmarz, W. Li, A. Genç, Y. Xia, L. Zheng, S. H. Lee, S.K. Karan, et al., Defect-engineering-stabilized $AgSbTe_2$ with high thermoelectric performance, Adv. Mater. 35 (11) (2023): 2208994.

[45] M. Hong, Z.-G. Chen, L. Yang, Z.-M. Liao, Y.-C. Zou, Y.-H. Chen, S. Matsumura, J. Zou, Achieving $zT > 2$ in p-type $AgSbTe_{2-x}Se_x$ alloys via exploring the extra light valence band and introducing dense stacking faults, Adv. Energy Mater. 8 (9) (2018): 1702333.

[46] Z.W. Chen, X.Y. Zhang, Y.Z. Pei, Manipulation of phonon transport in thermoelectrics, Adv. Mater. 30 (17) (2018): 1705617.

[47] Z. Chen, Z. Jian, W. Li, Y. Chang, B. Ge, R. Hanus, J. Yang, Y. Chen, M. Huang, G. J. Snyder, Y. Pei, Lattice dislocations enhancing thermoelectric PbTe in addition to band convergence, Adv. Mater. 29 (23) (2017): 1606768.

[48] Y. Wu, Z. Chen, P. Nan, F. Xiong, S. Lin, X. Zhang, Y. Chen, L. Chen, B. Ge, Y. Pei, Lattice strain advances thermoelectrics, Joule 3 (5) (2019) 1276–1288.

[49] C. Hu, K. Xia, C. Fu, X. Zhao, T. Zhu, Carrier grain boundary scattering in thermoelectric materials, Energy Environ. Sci. 15 (4) (2022) 1406–1422.

[50] K.Q. Zhang, S. Liu, X.C. Wang, S. Wu, Q.H. Xiong, X. Wang, J.Q. Chen, G.W. Wang, B. Zhang, H.X. Fu, et al., Dual alloying enables high thermoelectric performance in $AgSbTe_2$ by manipulating carrier transport behavior, Adv. Funct. Mater. 34 (34) (2024): 2400679.

[51] M. Liu, X. Zhang, Y. Wu, Z. Bu, Z. Chen, W. Li, Y. Pei, Screening metal electrodes for thermoelectric PbTe, ACS Appl. Mater. Interfaces 15 (4) (2023) 6169–6176.

[52] Z. Bu, X. Zhang, Y. Hu, Z. Chen, S. Lin, W. Li, C. Xiao, Y. Pei, A record thermoelectric efficiency in tellurium-free modules for low-grade waste heat recovery, Nat. Commun. 13 (1) (2022) 237.

[53] Z. Bu, X. Zhang, Y. Hu, Z. Chen, S. Lin, W. Li, Y. Pei, An over 10% module efficiency obtained using non-Bi_2Te_3 thermoelectric materials for recovering heat of <600 K, Energy Environ. Sci. 14 (12) (2021) 6506–6513.

[54] S. Lin, L. Guo, X. Wang, Y. Liu, Y. Wu, R. Li, H. Shao, M. Jin, Revealing the promising near-room-temperature thermoelectric performance in Ag_2Se single crystals, Journal of Materiomics 9 (4) (2023) 754–761.

[55] B.-C. Chen, K.-K. Wang, H.-J. Wu, Cation modulation in $AgSbTe_2$ realizes carrier optimization, defect engineering, and a 7% single-leg thermoelectric efficiency, Small 20 (36) (2024): 2401723.

[56] D. Kraemer, J. Sui, K. McEnaney, H. Zhao, Q. Jie, Z.F. Ren, G. Chen, High thermoelectric conversion efficiency of MgAgSb-based material with hot-pressed contacts, Energy Environ. Sci. 8 (4) (2015) 1299–1308.

[57] J.-W. Li, Z. Han, J. Yu, H.-L. Zhuang, H. Hu, B. Su, H. Li, Y. Jiang, L. Chen, W. Liu, et al., Wide-temperature-range thermoelectric n-type $Mg_3(Sb,Bi)_2$ with high average and peak zT values, Nat. Commun. 14 (1) (2023) 7428.

[58] L. Yin, C. Chen, F. Zhang, X. Li, F. Bai, Z. Zhang, X. Wang, J. Mao, F. Cao, X. Chen, et al., Reliable N-type $Mg_{3.2}Sb_{1.5}Bi_{0.49}Te_{0.01}$/304 stainless steel junction for thermoelectric applications, Acta Mater. 198 (2020) 25–34.
[59] H.-L. Zhuang, J. Pei, B. Cai, J. Dong, H. Hu, F.-H. Sun, Y. Pan, G.J. Snyder, J.-F. Li, Thermoelectric performance enhancement in BiSbTe alloy by microstructure modulation via cyclic spark plasma sintering with liquid phase, Adv. Funct. Mater. 31 (15) (2021): 2009681.
[60] H. Zhu, R. He, J. Mao, Q. Zhu, C. Li, J. Sun, W. Ren, Y. Wang, Z. Liu, Z. Tang, et al., Discovery of ZrCoBi based half Heuslers with high thermoelectric conversion efficiency, Nat. Commun. 9 (1) (2018) 2497.
[61] M. Kubo, T. Itoh, K. Tokuda, J. Shan, K. Kitagawa, Fabrication of layered p-type $AgSbTe_2$-$(Bi,Sb)_2Te_3$ thermoelectric module and its performances, J. Jpn. Soc. Powder Powder Metall. 51 (1) (2004) 10–15.
[62] J. Zhou, Z. Chen, J. Luo, W. Li, Y. Pei, Gradient doping enables an extraordinary efficiency in thermoelectric $PbTe_{1-x}I_x$, Adv. Mater. 36 (31) (2024): 2405299.
[63] J. Jiang, H. Zhu, Y. Niu, Q. Zhu, S. Song, T. Zhou, C. Wang, Z. Ren, Achieving high room-temperature thermoelectric performance in cubic AgCuTe, J. Mater. Chem. A 8 (9) (2020) 4790–4799.
[64] P.-Y. Deng, K.-K. Wang, H.-Y. Sung, W.-W. Wu, H.-J. Wu, Liquid-like copper chalcogenide modulates electron donors in high-performance n-type PbTe thermoelectrics, Cell Reports Physical Science 4 (6) (2023): 101413.
[65] H. Shi, Y. Qin, B. Qin, L. Su, Y. Wang, Y. Chen, X. Gao, H. Liang, Z.-H. Ge, T. Hong, L.-D. Zhao, Incompletely decomposed In_4SnSe_4 leads to high-ranged thermoelectric performance in n-type PbTe, Adv. Energy Mater. 12 (42) (2022): 2202539.
[66] X. Qi, R. Xiong, B. Sa, X. Zhang, W. Li, Y. Pei, Efficient rhombohedral GeTe thermoelectrics for low-grade heat recovery, Materials Today Physics 45 (2024): 101466.
[67] F. Hao, P. Qiu, Y. Tang, S. Bai, T. Xing, H.-S. Chu, Q. Zhang, P. Lu, T. Zhang, D. Ren, et al., High efficiency Bi_2Te_3-based materials and devices for thermoelectric power generation between 100 and 300 °C, Energy Environ. Sci. 9 (10) (2016) 3120–3127.
[68] B. Qin, D. Wang, X. Liu, Y. Qin, J.-F. Dong, J. Luo, J.-W. Li, W. Liu, G. Tan, X. Tang, et al., Power generation and thermoelectric cooling enabled by momentum and energy multiband alignments, Science 373 (6554) (2021) 556–561.
[69] P. Ying, R. He, J. Mao, Q. Zhang, H. Reith, J. Sui, Z. Ren, K. Nielsch, G. Schierning, Towards tellurium-free thermoelectric modules for power generation from low-grade heat, Nat. Commun. 12 (1) (2021) 1121.
[70] Z. Liu, N. Sato, W. Gao, K. Yubuta, N. Kawamoto, M. Mitome, K. Kurashima, Y. Owada, K. Nagase, C.-H. Lee, et al., Demonstration of ultrahigh thermoelectric efficiency of ~7.3% in Mg_3Sb_2/MgAgSb module for low-temperature energy harvesting, Joule 5 (5) (2021) 1196–1208.